ICOS INWIRE

ICOS improved sensors, network and interoperability for GMES

D6.2

Report on Coordinated network design over Europe with mesoscale models

C. Gerbig, U. Karstens, T. Koch, P. Kountouris (MPG)

Antoon Meesters, Han Dolman (VUA)

Gregoire Broquet (CEA)

ICOS-INWIRE (GA n°313169)

Document for public

Version 1.0, March 2015

www.icos-inwire.lsce.ipsl.fr

| | Deliverable: | **D6.2, Report on Coordinated network design over Europe with mesoscale models** |

	Deliverable:	**D6.2, Report on Coordinated network design over Europe with mesoscale models**
	Author(s):	**C. Gerbig, U. Karstens, T. Koch, P. Kountouris (MPG)** **Antoon Meesters, Han Dolman (VUA)** **Gregoire Broquet (CEA)**
	Date:	**07/05/2015**
	Activity:	**WP6: Towards interoperability between the European ICOS network and other GHG networks**
	Lead Partner:	**MPG**
	Document Issue:	**1.0**
	Dissemination Level:	**Public (PU)**
	Contact:	**Project Office ICOS-INWIRE:** **Nadine Schneider, LSCE, France** **nadine.schneider@lsce.ipsl.fr** **Tel +33 - 69 08 - 71 24**

	Name	**Partner**	**Date**
From	Ute Karstens	MPG	25/03/2015
Reviewed by	Jean-Daniel Paris	CEA/LSCE	7/05/2015
Approved by	Nadine Schneider	CEA/LSCE	8/5/2015

ABSTRACT

A coordinated network design study for Europe was performed using three different regional inversion systems for the estimation of biosphere-atmosphere exchange fluxes. Uncertainties for prior fluxes and model-data mismatch were harmonized to assure the inter-comparability of the inversion results. The prior error structure was based on a comparison of the different prior fluxes used in the inversions with eddy covariance observations. Uncertainty reductions in biosphere-atmosphere exchange fluxes were computed by the different inversion systems for the current and planned ICOS network of atmospheric stations, as well as for a hypothetic network with a gap in the area of Germany.

Inversion results show a strong spatial inhomogeneity in the uncertainty reductions with typical values for seasonal fluxes around 30-50% near observing sites for the pixel scale (50 km), and around 50% for national scales. While the general level of uncertainty reduction differs between the inversion systems, the increase of uncertainty reduction with increasing number of stations per area or country is similar.

TABLE OF CONTENTS

1 INTRODUCTION

1.1 Scope and objectives of the document

As new ICOS atmospheric monitoring stations are being set up, the choice of a measurement location has impact on the uncertainties of the estimated fluxes in the context of atmospheric transport inversions. Thus guidance from inverse modellers is needed such that the network can grow in a way that maximises the information content in retrieved GHG fluxes, or in specific targeted quantities such as national annual total biosphere-atmosphere exchange of CO_2. However, given the advanced state of the network development, and given the situation that typically other constraints such as logistics (site access, power, communication) and the fact that often pre-existing structures are used as tall towers, the decision was made to assess the ICOS network as it is planned, and address a set of related questions: what is the amount of information gained by a given network, by individual stations, and what is the impact of spatial gaps in the observing network. Providing such information to the ICOS atmospheric community will substantiate the importance of the network, and should encourage stakeholders to continue the development of the network.

This study focuses on regional (mesoscale) inversions, and on CO_2, since a parallel study undertaken in InGOS Task 15.7 "Network analysis and optimization" was related to N_2O and CH_4 inversions. Also the focus is limited to biosphere-atmosphere exchange, as current inversion systems are not yet capable for estimation of fossil fuel emissions of CO_2 based on data from the ICOS network.

The aim of the study is to provide insight on the uncertainty reduction using three mesoscale inversion systems with different transport models, but similar a priori flux error structure, similar selection of observations, and similar assumptions on transport model and measurement errors. Furthermore, the study aims to assess the impact of gaps in the measurement network. An overview of the three mesoscale inversion systems is given in Table 1. The inversion systems differ in their transport representation, prior flux, and optimization technique.

Table 1: Mesoscale inversion systems used in this study.

Partner	Transport	Transport resolution (deg)	Prior flux	Optimization
MPG	STILT/TM3	0.25	VPRM	4DVar
CEA/LSCE	CHIMERE	0.5	ORCHIDEE	4DVar
VUA	RAMS	0.5	5PM	Ensemble Kalman Filter

1.2 Structure of the document

Section 2 gives an overview of the assessment, with section 2.1 giving a short introduction on the mathematics of Bayesian inversions, section 2.2 providing an overview of the inversion systems used for this study, section 2.3 describing the joint protocol that was used to harmonize the simulations made by the different partners/inversion systems, and section 2.4 presenting the results in terms of uncertainty reduction in biosphere-atmosphere exchange fluxes for different observational network configurations. Section 3 provides the conclusions.

2 ASSESSMENT OF UNCERTAINTY REDUCTION

2.1 Basics on inversions and uncertainty reduction

Atmospheric inversions use observed time series of atmospheric mixing ratios from a network of stations in combination with a transport model to infer optimal fluxes, i.e. fluxes that result in simulated mixing ratios that are optimally close to the observations. They rely on the Bayesian update of a prior guess for the fluxes. This can be expressed in a cost function J that needs to be minimized:

$$J = (Hx - y)^T C_y^{-1}(Hx - y) + \left(x - x_p\right)^T C_p^{-1}\left(x - x_p\right) \tag{1}$$

Here y is the vector of observed mixing ratios at different times and locations, H is the transport model (as the transport is linear for conserved tracers, H is a matrix), x is the vector of fluxes at all different times (e.g. hourly) and locations (e.g. every 0.5 degree lat/lon), x_p is the a priori guess for the fluxes, and C_y and C_p are the model-data mismatch uncertainty (due to the discrete representation of the fluxes, to the transport model and to the measurement errors) and the prior uncertainty, respectively, written as covariance matrices due to the assumption that these uncertainties have Gaussian distributions. Note that the vector x is often called "control vector", as it contains all adjustable elements controlling the biosphere-atmosphere exchange fluxes. The cost function thus consists of one term describing the model-data mismatch and one term describing the mismatch between flux and prior flux. Minimizing this leads to the posterior estimate for the fluxes:

$$x_{post} = \left(H^T C_y^{-1}H + C_p^{-1}\right)^{-1}\left(H^T C_y^{-1}y + C_p^{-1}x_p\right) \tag{2}$$

This is a weighted sum of the constraint on the fluxes by the data and the prior flux, where the weights correspond to the uncertainties. For the uncertainty in the posterior fluxes, one obtains:

$$C_{post} = \left(H^T C_y^{-1}H + C_p^{-1}\right)^{-1} \tag{3}$$

This uncertainty depends on the transport, which decides how strongly the flux elements have been "seen" by the observation locations (H contains in each row the "footprint", i.e. the sensitivity of mixing ratio observation to upstream fluxes). The posterior uncertainty also depends on the uncertainties for model-data mismatch and prior fluxes. It does not depend on the prior fluxes, and also not on the observations, but only on the locations and times where and when the observations were made (specified through the first term of equation (1) describing the observational constraint).

To relate the estimated surface flux fields to individual targeted quantities (e.g. national annual totals), we can define an aggregation scalar operator W, such that $F_{post}=Wx_{post}$ corresponds for example to the annual mean flux, averaged over a given national domain. Similarly, the full error covariance matrix C_{post} of posterior fluxes can be aggregated to the standard deviation of the posterior uncertainty $\sigma_{F,post}$ in the target quantity:

$$\sigma_{F,post} = \sqrt{W\,C_{post}\,W^T} \qquad (4)$$

Uncertainty reduction U is typically defined as the relative reduction of the posterior relative to the prior uncertainty for a given target quantity:

$$U = (\sigma_{F,prior} - \sigma_{F,post})/\sigma_{F,prior} \qquad (5)$$

For network assessments, the posterior uncertainty or the uncertainty reduction of different candidate networks can be used to assess their potential. It is obvious that the resulting uncertainty reduction for a target quantity at a scale larger than that of the control vector strongly depends on the off-diagonal elements of the C_p and C_{post} matrices, i.e. on the correlation of uncertainties in fluxes in the control vector at different locations or different times. Note that for areas not "seen" by the network, i.e. where the footprint is zero, there is formally no potential for atmospheric measurements to constrain fluxes, except if appropriate spatial or temporal correlations exist in the a priori uncertainty, fluxes in such areas appear to be indirectly constrained by directly constrained (and error-correlated) fluxes elsewhere. In other words, as the adjustments to the fluxes have a grain-size corresponding to the spatiotemporal correlation length, fluxes in areas with gaps in the footprints can be constrained as long as the grain-size is sufficiently large. Thus specifying the spatiotemporal correlation of errors is crucial, as it spreads the information on top of what is given by atmospheric transport alone. On the other hand, the number of unknowns (wall-to-wall fluxes with a high spatial and temporal resolution) easily exceeds the number of observations (hourly time series at each network site), which means that the problem is underdetermined. Thus the smoothing and extrapolation provided by spatiotemporal correlations in the a priori error helps constraining fluxes beyond the near vicinity (footprint) of stations.

2.2 Inversion systems used

2.2.1 Inversion system partner MPG

For the inversions we deployed the 2-step inversion scheme (R3), which allows for sequentially performing a global inversion followed by a regional inversion, where the transport models and flux models used for the different domains can be different. Here the STILT-TM3 inversion system was used, combining the global TM3 model driven by NCEP wind fields with the regional STILT model driven by ECMWF short-term forecast fields (R4). The regional model domain (Fig. 1) includes most of Europe.

The control space corresponds to NEE fluxes, such that the system solves for corrections to the a priori NEE fluxes. The optimization scheme is an iterative matrix inversion, comparable to typical 4D-variational schemes used in weather prediction.

To derive posterior uncertainties, the inversion system uses a Monte Carlo method, where 40 ensembles of realizations of prior error and model-data mismatch errors are generated, and the inversion is repeated for each ensemble member, resulting in posterior fluxes that exhibit a spread corresponding to the posterior uncertainty.

2.2.2 Inversion system partner VUA

The VUA inversion system uses RAMS (the Regional Atmospheric Modelling System) as transport model. This weather prediction model with capability for tracer transport is run forward for an ensemble of flux realizations (created using realizations of prior error) and realizations of model-data mismatch error, and creates this way an ensemble of synthetic observations.

Inversions are performed only for periods of three months: MAM, JJA and SON 2007, to prevent unmanagable flux covariance matrices. The control space consists of scaling factors for GPP and respiration for each cell-month combination, and one bias factor (multiplied with the respiration flux) for the whole season and domain. For the control vector, an ensemble of 100 random members is set up, whose statistics satisfy the protocol (section 2.3). Forward runs with RAMS yield "observations" for each member. Inversion is done with an ensemble Kalman filter (EKF), which processes the central concentrations station-by-station, thus transforming step-by-step the prior to a posterior flux ensemble (R5). From this, flux variances and other statistics are straightforwardly calculated.

Since the ensemble has the imposed statistical properties only in approximation, relations between the variations in the fluxes and concentrations may occur not only by causality, but also by coincidence, causing spurious "improvements" of the fluxes when the EKF is applied. Several measures were taken to correct for this:

(1) Earlier observations are not allowed to improve later fluxes;
(2) Observations are not allowed to improve fluxes more than 1000 km away ("localization").
(3) An adjustment brought about by an observation is only accepted if it reduces the scaling-factor's standard deviation by at least 5 % ("dynamic localization", see R6).

Unfortunately, (3) creates a spurious dependence of the results on the order in which the observations (stations) are processed. This dependence is quite weak for small station numbers, but it becomes strong with many stations, with late stations having a smaller impact than early ones. To overcome this difficulty, five "reference locations" were defined, being the four corners and the centre of Germany. For each reference location, a complete inversion is done, with the stations ordered with increasing distance to the reference location. After all inversions are finished, for each pixel, the best of the 5 flux error reductions is chosen as final result.

2.2.3 Inversion system partner CEA

The system used at CEA/LSCE has been described in details in Broquet et al. (R7 and R8). It consists in a variational framework which uses a Europe 0.5° resolution configuration of the Eulerian CHIMERE transport model and which controls NEE fluxes at 6-hour and 0.5° resolution during a 1-year period. The fluxes are optimized through the minimization of the cost function J (equation 1) using an iterative gradient technique. During each iteration, the adjoint code of CHIMERE is used to compute the gradient of the cost

function. The posterior uncertainties are computed based on a Monte Carlo framework with ensemble experiments such as for the system from MPG (see section 2.2.1).

For the experiments in this project, CHIMERE is driven by ECMWF meteorological forcing for the year 2007 and its domain is extended to 12°W-35°E / 35°N-62°N. The control vector is extended for including an annual bias on NEE (see section 2.3).

Note that due to severe problems with the computing facilities that the LSCE system utilizes, it was not yet possible to provide results for this study. It is the plan to update this report by including results before the end of the ICOS Inwire project.

2.3 Joint protocol for regional inversions

2.3.1 Observational networks

This study focuses on existing and planned atmospheric stations within ICOS. ICOS current and future stations were taken from the ICOS Stakeholders Handbook 2012 (R1) and 2013 (R2). Some additional stations were added from the InGOS network design study station set 3 (PTR, HUN, WEY). All locations were updated using Google-earth. The overview of the network is given in Fig. 1.
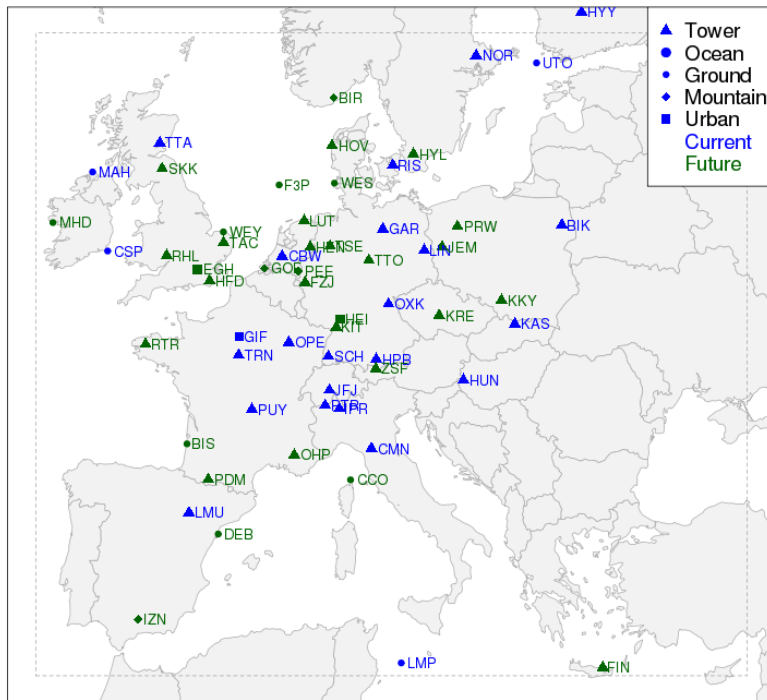

Figure 1: Network with current (blue) and future (green) ICOS atmospheric sites used for Task 6.2. Also shown is the domain over which inverse results were compared between the different inversion systems (dashed grey lines).

Out of these stations, three station sets were formed:

- Set 1: current ICOS network **(25 Stations)**
- Set 2: current + future ICOS network **(25+33=58 Stations)**

- Set 3: Gap analysis (omitting all observations in Germany) **(25+33-12=46 Stations)**

A station list with information on location, inlet height, and in which of the three stations sets the station is included in was sent out by partner MPG to the other participants.

For mountain stations, the model level representing the inlet height of the observations is ambiguous because of the possibly poor resolution of the orography in the vicinity of mountains. With the resolution used in the transport models used for the inversion systems, the terrain height has to be taken into account to some degree. The systems therefore use the model-level that is at inlet height plus 3/10 (VUA), 5/10 (STILT) and 10/10 (LSCE) of the difference of true terrain height and model terrain height.

A common model domain for comparing the flux retrievals was chosen with the south-west corner at 35°N, 11°W and the north-east corner at 61°N, 35°E. All flux retrievals focused on the year 2007.

2.3.2 Prior error setup

Prior uncertainties for different inversions should be consistent regarding the error structure and the uncertainty for annually and spatially integrated biosphere-atmosphere flux within the domain of interest. The following error structure was derived from comparison to flux observations at ecosystem sites and based on the ICOS-Inwire MS18 report on the "Assessment of a priori error structure", which details the prior error structure in terms of temporal and spatial correlation and in terms of the local standard deviation. MS18 used comparisons of eddy covariance flux observations with simulated fluxes from the three different models used to generate prior fluxes for the inversion systems deployed here. Initial assessments of the resulting uncertainty budget for annually and domain-wide integrated fluxes suggest additional degrees of freedom to adjust large-scale and long-term mismatch that is not captured by the analysis presented in MS18.

For temporal correlation, the analysis of model-data differences is consistent with a time scale of about 40 days (see Fig. 2). The STILT-TM3 system uses a temporal correlation that corresponds to an exponential decay with a time scale of 33 days. The VUA system uses a time resolution of 1 month, and temporal correlations for lag-times longer than that are represented by a polynomial function (see also the blue line in Fig. 2).

The spatial correlation analysis of model-data differences resulted in correlation length scales of 30-40 km, while differences between models showed larger spatial correlation lengths. Therefore a slightly larger value of 50 km spatial correlation scale was suggested in the protocol. The different scales used by the different inversion systems are given in Table 2. Diagonal elements of the prior error covariance were taken to be consistent with the analysis of flux model – eddy covariance differences, scaled down to account for the difference in spatial resolution of the control vector (c.f. R9).
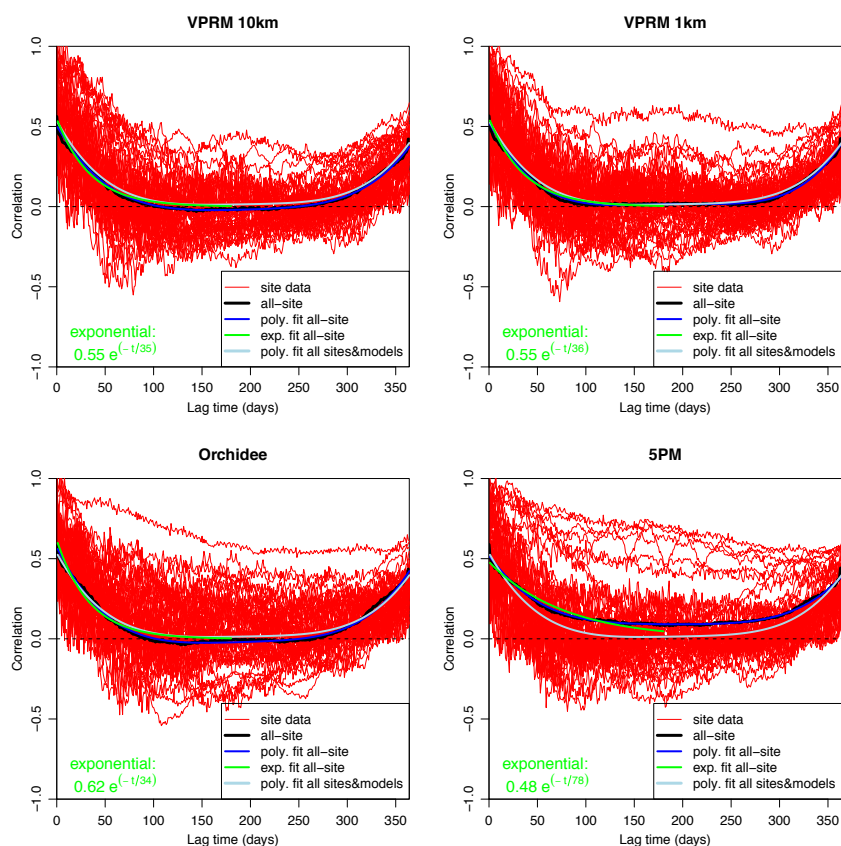
Figure 2: Temporal correlations of model-data differences for the different biosphere models used for prior fluxes as function of lag time.

The prior uncertainty for annually and domain wide integrated fluxes was harmonized for each inversion system to match with the typical differences of budgets from six different process models (www.carboscope.eu). Those resulted in a standard deviation of 0.36 GtC/a for the Transcom EU region; scaling this to the land area for the domain used here this corresponds to 0.2 GtC/a. Aggregating above specified spatiotemporal error covariance matrices to annual and EU wide scale leaves for the long-term bias an uncertainty listed under "LTB" in Table 2.

Table 2: Prior uncertainty parameters used in the different inversion systems. LTB refers to the choice made for including additional degrees of freedom for a long-term bias component.

Inversion system	Control vector	Temporal scale (days)	Spatial scale meridional/zonal (km)	Diagonal (μmoles/m^2/s)	LTB (GtC/a)
STILT-TM3	NEE	33 (exp)	33/66	2.3	0.103
VUA	GEE/RESP scaling	40 (poly)	50/50	2.0	0.171
CEA	NEE	33.7 (exp)	50/50	2.3	0.156

Note that the implementation of the harmonized uncertainties was specific for each regional inversion system, as they use different control spaces (i.e. the flux variables that

the systems optimize). STILT-TM3 uses an additive correction to the prior NEE for every 0.5x0.5 degree surface pixel, while the VUA system uses scaling factors for GEE (gross ecosystem exchange) and respiration for every surface pixel with a size of 50 km. Also the implementation of the long-term bias (LTB) component is different between the different systems. The VUA system uses a bias component consisting of seasonal factors that scale respiration fluxes from the 5PM flux model, while the STILT-TM3 and LSCE systems use respiration fluxes from the VPRM and ORCHIDEE flux model, respectively, but each scaled with single (annual) factors. Note however that the resulting uncertainty of the annual LTB is larger for the VUA and LSCE systems compared to STILT-TM3.

2.3.3 Model-data mismatch error setup

The model-data mismatch errors in Table 3 are used as representative for current inverse modelling systems. The uncertainties are effective uncertainties for 1 week observing period, i.e. there is additional error inflation to account for the fact that model-data mismatch errors are not fully random noise, but that they are correlated typically over synoptic time scales. With e.g. 14 observations per week (12:00 and 15:00 or 0:00 and 3:00 (mountain sites) observational times every day), the inflation factor is about 3.7 (the square root of the number of observations).

Table 3: Model-data mismatch for CO_2 for tall towers (T), ground stations (G), ocean/coastal stations (O), mountain stations (M), and urban polluted sites (UP).

	T	G	O	M	UP
weekly uncertainty (ppm)	3	5	3	3	8
Number of sites	28	7	11	9	3

2.3.4 Uncertainty reduction output

The following products were requested from the different inversion systems for joint analysis of the results:

- spatial maps of annually/seasonally integrated uncertainties (prior error, posterior error) for each station set (1-3), as netcdf files
- country aggregated tables for annually integrated prior and posterior uncertainties for each station set (1-3), as ascii files

In addition a description of the specific setup used for the inversion experiments was requested. Altogether this allowed for consistent generation of maps with uncertainty reduction.

All involved regional inversion systems are capable of providing posterior uncertainty estimates for their control vector (fluxes or controlling parameters) according to equation (3), or for targeted quantities according to equation (4). Subsequent analysis provides estimated posterior uncertainties for target quantities. Uncertainty reduction was then computed from the individual results for targeted quantities according to equation (5).

2.4 Results

2.4.1 Spatial distribution of uncertainty reduction

Uncertainty reduction was provided by partners VUA for different seasons except for winter, and by MPG for all seasons and for the full year 2007. Using the currently existing ICOS stations (set 1 with 25 stations), the uncertainty reduction for seasonal fluxes typically reaches values of around 50% and 30% in the vicinity of observing stations (Fig. 3). The average uncertainty reduction for land pixels only is 7.1% for STILT-TM3, while for the VUA system it is 19.5%. It is obvious that STILT-TM3 has a lower overall uncertainty reduction, which seems to drop stronger with distance to the stations. This is similar for the uncertainty reduction obtained for the future ICOS network (station set 2), but there the average uncertainty reduction for land regions is 11.4% and 23.4% for STILT-TM3 and VUA, respectively (see Fig. 4). This indicates that the addition of 33 stations in set 2 relative to set 1 provide an additional 4% reduction in uncertainty for pixel-resolved fluxes at seasonal time scales.

Note that the absolute level of uncertainty reduction is to a strong degree dependent on the prior uncertainties chosen for this assessment. The choice of a 0.2 GtC/a uncertainty for domain-wide annually integrated fluxes is smaller than what is typically used, resulting in uncertainty reduction that is lower compared to other inversions.

Seasonal differences are minor compared to the spatial differences and usually smaller compared to the differences for the different networks. However, STILT-TM3 shows on average 1-2% lower uncertainty reduction for summer, and about 2% larger uncertainty reduction for fall compared to spring. In contrast, the VUA system shows slightly (0.5-1%) larger uncertainty reduction for summer, and a stronger (6-7%) increase for fall compared to spring. Those differences are partially caused by the different transport models involved that control through their parameterization of vertical mixing (cloud venting, turbulent mixing in the boundary layer) the sensitivity of the network to upstream fluxes. Another cause for those seasonal differences might be the different treatment of the long-term bias component, which has seasonal flexibility in the VUA system, but not in STILT-TM3.
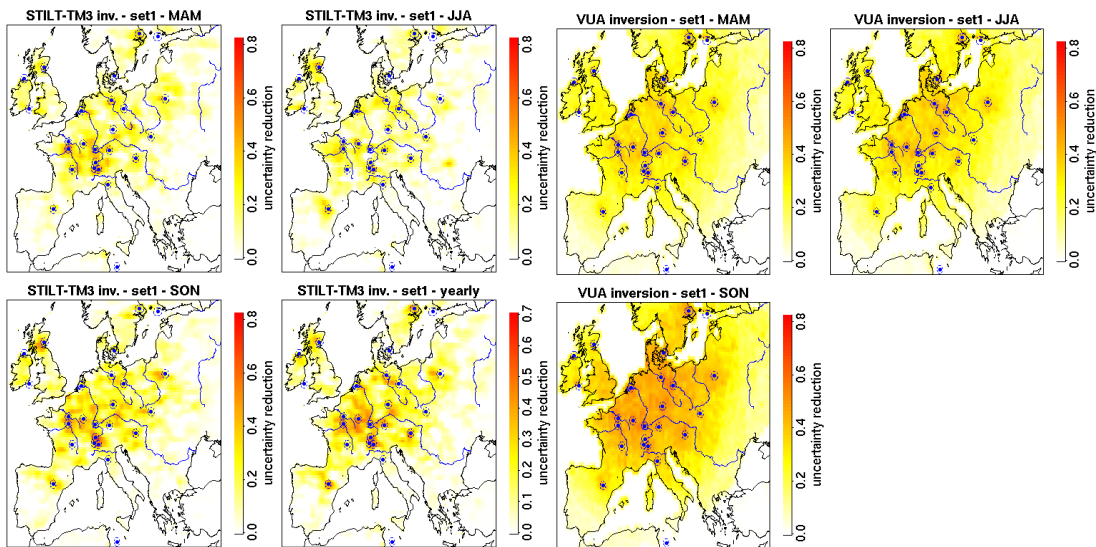
Figure 3: Uncertainty reduction maps for the current ICOS network (station set 1) for different seasons (MAM: months 3-5, JJA: months 6-8, SON: months 9-11) and for the full year 2007 for STILT-TM3 (left panels) and the VUA inversion system (right panels).
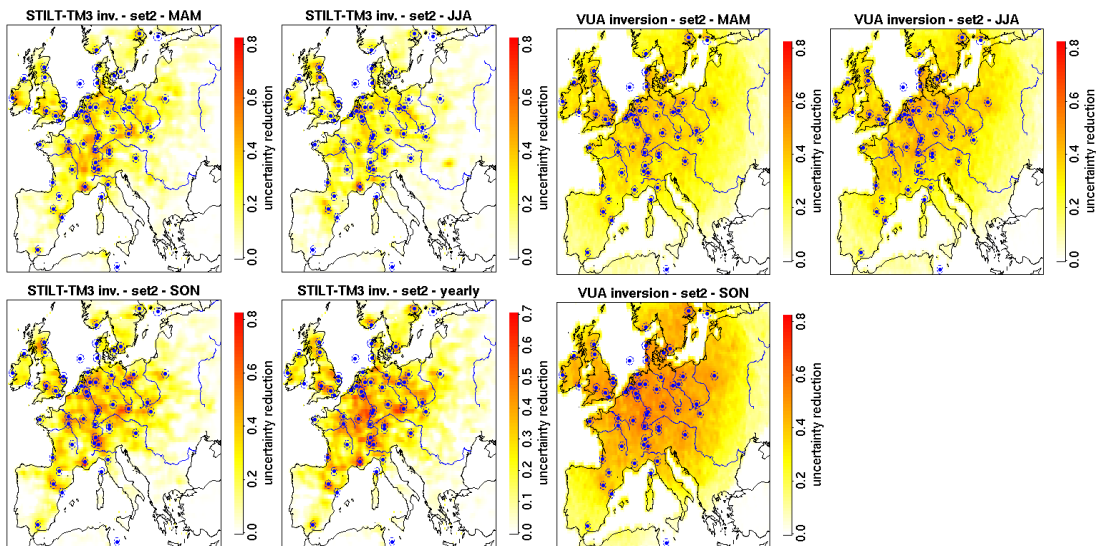

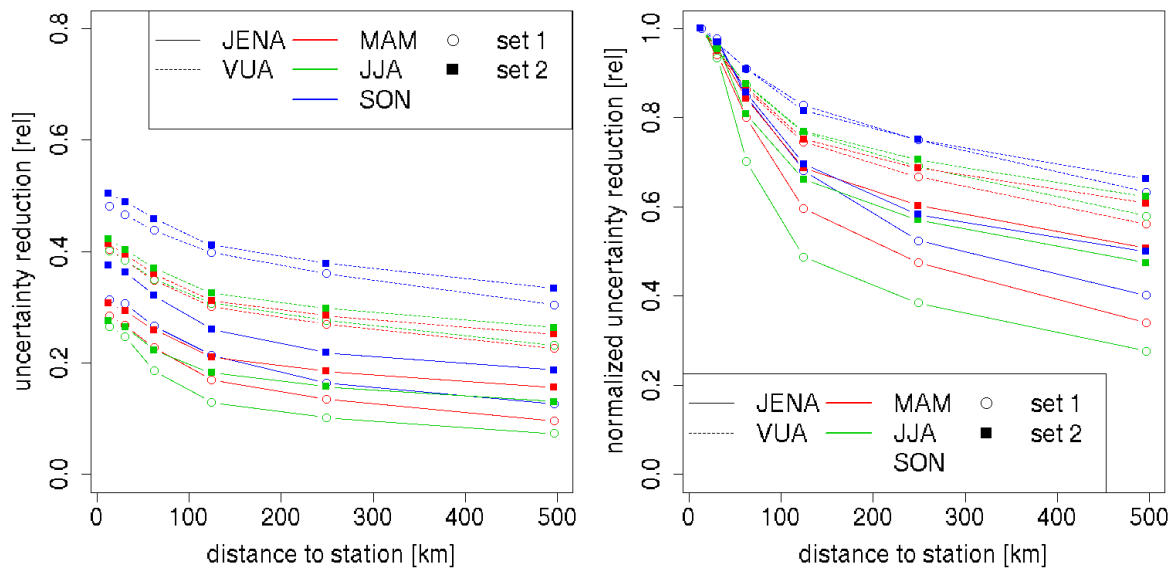**Figure 4:** as Fig. 3, but for the future ICOS network (station set 2).

Figure 5: Dependence of spatial pattern of uncertainty reduction on distance to the closest station for the different inversion systems, seasons, and station sets (1 and 2) (left), and the same quantity when normalizing to the respective uncertainty reduction at zero distance (right).

The different behaviour of the inversion systems is made clearer when the average uncertainty reduction for seasonal fluxes at pixel-level is analysed as function of distance to the closest atmospheric station (Fig. 5, left). A clear offset is visible between results from STILT-TM3 and the VUA system, with overall lower uncertainty reduction from the STILT-TM3 system. The relative drop in uncertainty reduction with distance from the stations (Fig. 5, right) is stronger for STILT-TM3, indicating a more localized effect.

Note that both systems use a comparable resolution for the control space, the same prior uncertainty for domain-wide integrated fluxes, and the same uncertainty for model-data mismatch. Differences are in the values for the prior uncertainty for the LTB, with larger values for the VUA system that result in correspondingly larger uncertainty reduction. Such large differences in the reduction of uncertainty could also related to either differences in the transport model deployed (which is highly unlikely), or to the specifics of the inversion systems optimization schemes. In fact, the EKF method deployed in the VUA system shows an artefact: Due to the limited number of members in the ensemble, the intended statistics is only imperfectly approximated, and this has as a consequence that sometimes a change in a flux may correspond to an improvement of an "observed" concentration by coincidence instead of by causation. This so-called "localization problem" causes the inversion system to somewhat exaggerate the error reduction in the long term. The problem is especially important with a large number of concentration sites, as is used here, because this causes an accumulation of small spurious contributions to error reduction. As described above, a number of measures were taken to reduce this effect, but there is some reason to think that the comparatively good results (i.e. overall large uncertainty reduction) of the EKF inversion are to some extent due to this effect.

2.4.2 Uncertainty reduction at the national scale

The inversion output was also used to produce uncertainty reduction for most of the EU27 countries (for those represented within the spatial domain, Fig. 1). Average uncertainty reduction for seasonally averaged fluxes are shown in Fig. 6 (left) for the regional inversion systems, together with results from the TM3 inversion system, which operates at coarse (4x5 deg.) spatial scales. The two regional inversion systems show clear patterns in uncertainty reductions for the different countries. It is obvious that a coarse global inversion system such as TM3 cannot capture these differences on sub-continental scales. The additional uncertainty reduction at national level when adding the 33 stations (set 2, Fig. 6, right) is also clearly seen. Despite of the overall larger uncertainty reduction obtained with the VUA system, it is reassuring to see that the patterns in uncertainty reduction at the national level are quite consistent between the two systems.
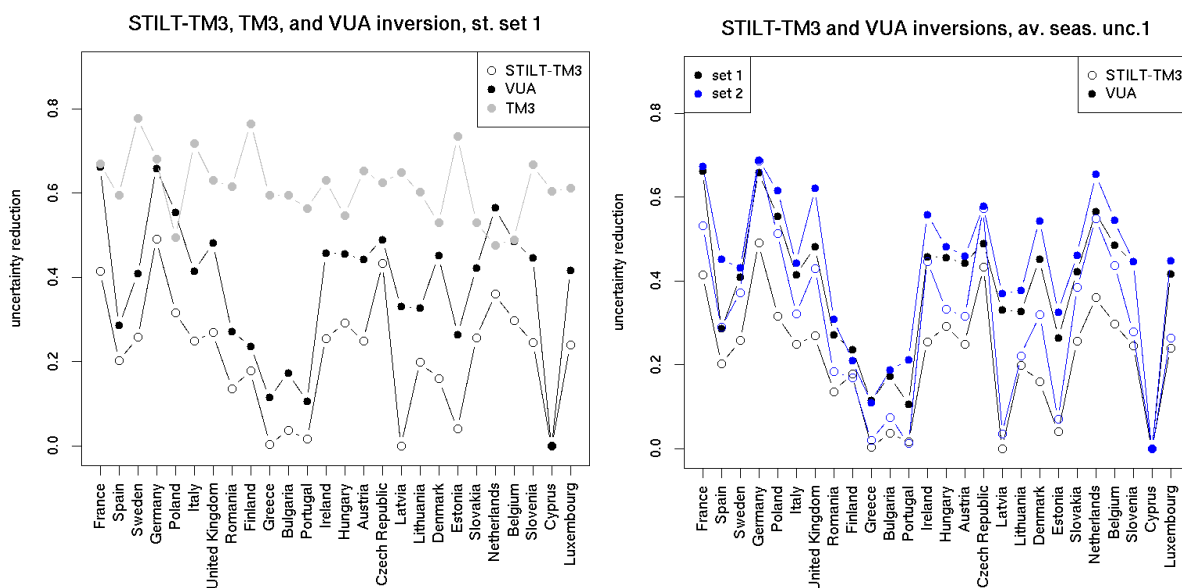

Figure 6: Uncertainty reduction for seasonally averaged fluxes for station set 1 (current ICOS) for the regional inversion systems STILT-TM3 and VUA, and for the TM3 global inversion system (left), and uncertainty reduction for current and future (set 2) ICOS network (right). The countries are ordered by their size.

An obvious question is whether the number of stations per country or the areal density of stations is a predictor of the uncertainty reduction at the country scale. Results from the regional inversion systems indicate this to some degree, as the uncertainty reduction for seasonal averaged fluxes increase with the number of observational sites per country and with the areal density (Fig. 7). However, a direct linear relationship cannot be established, likely due to the inhomogeneity of the network and due to the relatively low overall number of sites.
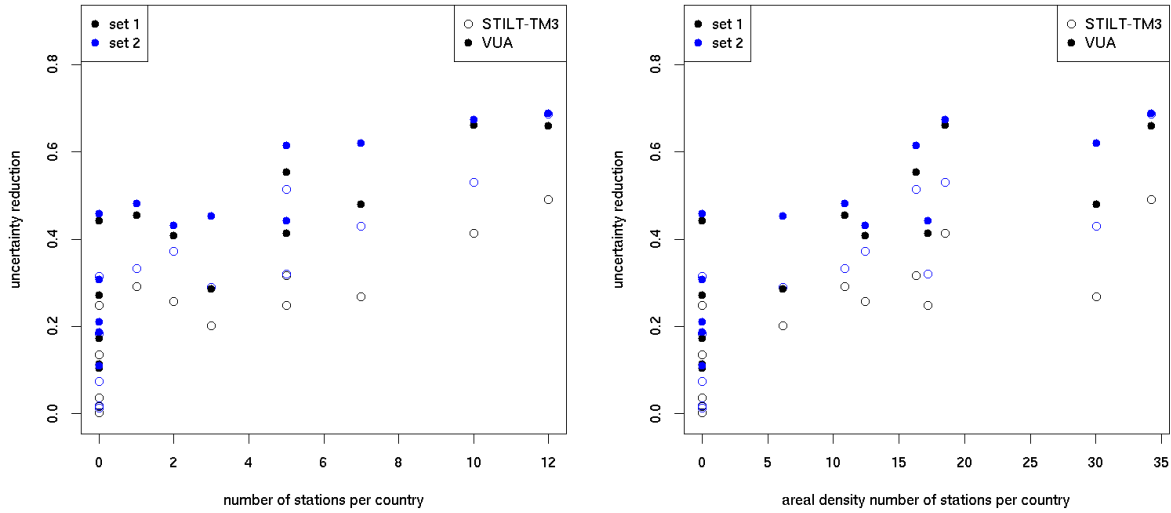
Figure 7: Uncertainty reduction for different countries as function of the number of observations per country, for station set 1 and 2 provided by the two regional inversion systems (left), and as function of the areal density of stations (unit: stations per Mio. square km) (right). Only countries with an area larger than 0.08 Mio square km (as represented within the domain shown in Fig. 1) are shown in the right figure.

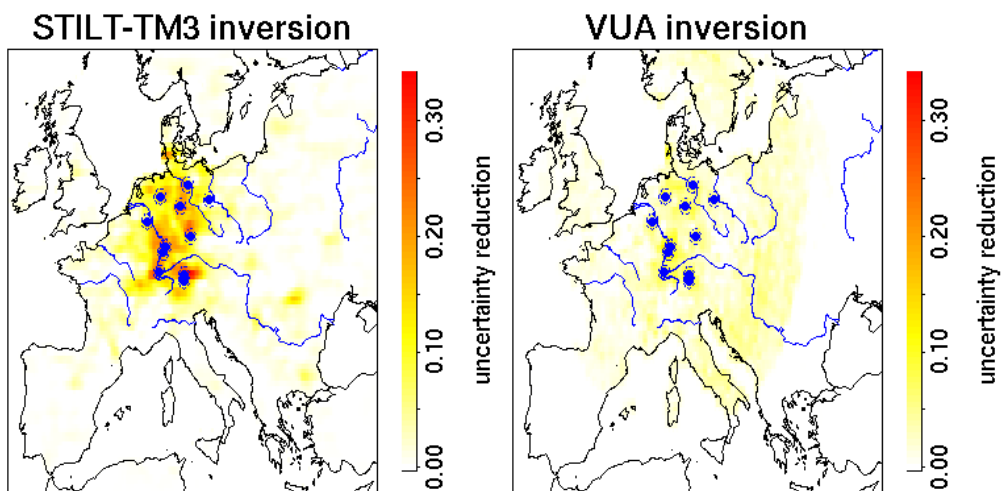## 2.4.3 Impact of network gap on reduction

Figure 8: Difference in uncertainty reduction for seasonally averaged fluxes between station sets 2 and 3, the latter of which has a gap in the network for Germany.

To assess the impact of a spatial gap in the network, uncertainty reduction was computed also for a network with stations missing in Germany. The impact is clearly visible in Fig. 8, where the uncertainty reduction is significantly reduced for the area of Germany. The impact is stronger and more localized for the STILT-TM3 inversion, which is in line with the previously mentioned more localized uncertainty reduction in the vicinity of observing stations.
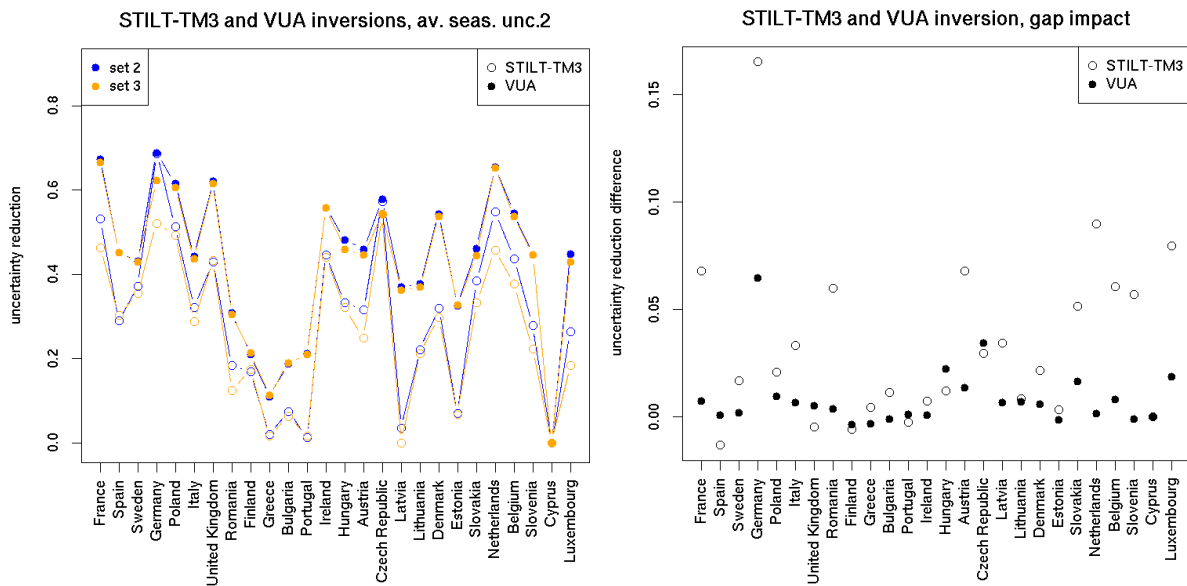
Figure 9: Uncertainty reduction for seasonally averaged fluxes for station sets 2 (future network) and 3 with a gap (left), and difference in uncertainty reduction for set 2 and set 3 showing the impact of a gap in the network for the area of Germany (right).

According to results from the STILT-TM3 system, the gap over Germany has direct impact on uncertainty reduction for Germany (decrease by 17%) (Fig. 9, right), which however remains quite high in comparison to other countries. The fact that the uncertainty reduction does not drop to smaller values is related to the impact of the network's strong coverage for countries around Germany. Correspondingly the network gap over Germany decreases the uncertainty reduction for neighbouring countries such as the Netherlands, Luxembourg, Austria, and France, but also for more distant countries such as Romania and Slovenia. A slightly opposite impact is found for Spain (increase by 1%), which is an indication of uncertainties due to a limited ensemble size in the Monte Carlo method applied to retrieve the posterior uncertainties. For the VUA system the network gap resulted in a smaller impact, with a decrease in uncertainty reduction by 6% for Germany, followed by the 3% decrease for the Czech Republic.

3 CONCLUSION

This coordinated network design study was made with three different regional inversion systems for the estimation of biosphere-atmosphere exchange fluxes. The study uses a strict protocol to control the observational networks used, and to harmonize the uncertainties used for model-data mismatch and prior fluxes. The a priori error structure was based on a comparison of the different a priori fluxes with eddy covariance observations (ICOS-INWIRE deliverable D6.1), which resulted in quite short spatial error correlation scales.

The results from the different inversion systems show a strong spatial inhomogeneity in the uncertainty reduction for seasonally or annually integrated fluxes, which is a consequence of the short prior error correlation scales. However, those scales are regarded as realistic, as they are based on a statistical analysis of differences between prior flux models and observations.

Typical uncertainty reductions for seasonal fluxes are around 30-50% near observing sites for the pixel scale (50 km), and around 50% for national scales. The regional inversion systems gave a similar answer regarding the pattern of uncertainty reduction at the national scale. A comparison to a coarse-resolution global inversion system clearly indicated that such regional systems are needed to provide information on sub-continental scales.

The overall uncertainty reduction is related to the tight prior error constraint (0.2 GtC/a uncertainty for domain-wide annually integrated fluxes), which we argue gives a more realistic picture for the potential of the network as compared to uncertainty reductions typically obtained for global inversion systems. Note however that model-data mismatch uncertainties are chosen that are typically used in current inversion systems, such that the observational constraint for future (improved) models is likely to increase.

Differences in the uncertainty reduction between the STILT-TM3 and the VUA inversion systems are partially related to the differing implementation of the long-term bias, resulting in larger prior uncertainty for the LTB for VUA, but could also reflect differences in optimization approach. A problem worth attention is the spurious amount of error reduction ("localization problem") to which the EKF is prone, in spite of the applied corrections. When data from many concentration stations are being used, as is the case in the present exercise, there is a growth not only of the real but also of the spurious reduction. The comparatively strong error reduction found with the EKF method may be an interesting illustration of this artefact. Unfortunately, the size of the effect is difficult to quantify with the available means. Another problem, typical for the use of an Ensemble Kalman Filter for many concentration stations, is a slight dependence on the order in which those stations are processed. A well-working remedy was devised for this problem.

The assessment indicates that the density of stations is a critical parameter in obtaining a homogeneous uncertainty reduction in surface-atmosphere exchange fluxes. Uncertainty reduction increases with increasing number of stations per country or area. Analysis of a

hypothetical network with a gap in the area of Germany indicates a significant impact for the immediate area, but also shows influence on uncertainty reduction for neighbouring countries. The fact that the gap was assumed to be in a central location of the network, with many stations around, mediated the impact to a certain degree. However for countries located at the edge of the network this is not expected to occur to such a degree. For the development of the ICOS atmospheric network this means that it is crucial to expand into currently under-sampled regions, especially Southern and Eastern Europe.

4 REFERENCES

R 1 ICOS Stakeholders Handbook, 2012

R 2 ICOS Stakeholders Handbook, 2013

R 3 Rödenbeck, C., Gerbig, C., Trusilova, K. and Heimann, M.: A two-step scheme for high-resolution regional atmospheric trace gas inversions based on independent models, Atmos. Chem. Phys., 9(14), 5331–5342, 2009.

R 4 Trusilova, K., Roedenbeck, C., Gerbig, C. and Heimann, M.: Technical Note: A new coupled system for global-to-regional downscaling of CO2 concentration estimation, Atmos. Chem. Phys., 10(7), 3205–3213, 2010.

R 5 Peters, W., MILLER, J. B., Whitaker, J., Denning, A. S., Hirsch, A., Krol, M. C., Zupanski, D., Bruhwiler, L. and TANS, P. P.: An ensemble data assimilation system to estimate CO 2surface fluxes from atmospheric trace gas observations, J. Geophys. Res., 110(D24), D24304, doi:10.1029/2005JD006157, 2005.

R 6 Zupanski, D., Denning, A. S., Uliasz, M., Zupanski, M., Schuh, A. E., Rayner, P. J., Peters, W. and Corbin, K. D.: Carbon flux bias estimation employing Maximum Likelihood Ensemble Filter (MLEF), J. Geophys. Res., 112(D17), D17107, doi:10.1029/2006JD008371, 2007.

R 7 Broquet, G., Chevallier, F., Rayner, P., Aulagnier, C., Pison, I., Ramonet, M., Schmidt, M., Vermeulen, A. T. and Ciais, P.: A European summertime CO 2biogenic flux inversion at mesoscale from continuous in situ mixing ratio measurements, J. Geophys. Res., 116(D23), doi:10.1029/2011JD016202, 2011.

R 8 Broquet, G., Chevallier, F., Bréon, F. M., Kadygrov, N., Alemanno, M., Apadula, F., Hammer, S., Haszpra, L., Meinhardt, F., Morguí, J. A., Necki, J., Piacentino, S., Ramonet, M., Schmidt, M., Thompson, R. L., Vermeulen, A. T., Yver, C. and CIAIS, P.: Regional inversion of CO2 ecosystem fluxes from atmospheric measurements: reliability of the uncertainty estimates, Atmos. Chem. Phys, 13(17), 9039-9056, doi:10.5194/acp-13-9039-2013, 2013.

R 9 Chevallier, F., Wang, T., Ciais, P., Maignan, F., Bocquet, M., Altaf Arain, M., Cescatti, A., CHEN, J., Dolman, A. J., Law, B. E., Margolis, H. A., Montagnani, L. and Moors, E. J.: What eddy-covariance measurements tell us about prior land flux errors in CO 2-flux inversion schemes, Global Biogeochem. Cycles, 26(1), doi:10.1029/2010GB003974, 2012.

5 DEFINITIONS, ACRONYMS AND ABBREVIATIONS

Acronym	Long name
CHIMERE	A multi-scale model for air quality forecasting and simulation
ECMWF	European Centre for Medium-Range Weather Forecasts
EKF	Ensemble Kalman Filter
ICOS	Integrated Carbon Observing System
InGOS	Integrated non-CO_2 Greenhouse gas Observing System
LSCE	Le Laboratoire des Sciences du Climat et de l'Environnement
MPG	Max Planck Gesellschaft (Max Planck Society)
MPI-BGC	Max Planck Institute for Biogeochemistry
NEE	Net Ecosystem Exchange
RAMS	Regional Atmospheric Modelling System
STILT	Stochastic Time-Inverted Lagrangian Transport
TM3	The global transport model used at MPI-BGC
VPRM	Vegetation Photosynthesis and Respiration Model
VUA	Vrije Universiteit Amsterdam
WMO	World Meteorological Organisation